Facile synthesis of highly fluorescent free-standing films comprising of graphitic carbon nitride (g-C_3N_4) nanolayers

Ram Manohar Yadav[a,b] *, Rajesh Kumar[c], Amir Aliyan[d], Pramod S. Dobal [a], Santoshkumar Biradar[b], Robert Vajtai[b,e], Dinesh Pratap Singh[f], Angel A. Martí[b,d,*] and Pulickel M. Ajayan [b,d,*]

[a] Department of Physics, VSSD College Kanpur, India-208002

[b] Department of Materials Science and NanoEngineering, Rice University, Houston, TX, USA-77005

[c] Department of Electrical and Electronic Information Engineering, Toyohashi University of Technology, 1-1 Hibarigaoka, Tempaku-cho, Toyohashi, Aichi, 441-8580, Japan

[d] Department of Chemistry, Rice University, Houston, TX, USA-77005

[e] Interdisciplinary Excellence Centre, Department of Applied and Environmental Chemistry, University of Szeged, Rerrich Béla tér 1, Szeged, Hungary

[f] Department of Physics, University of Santiago, Santiago-9170124, Chile

Abstract

Astounding graphitic carbon nitride (g-C_3N_4) nanostructures have attracted huge attention due to their unique electronic structures, suitable band gap, thermal and chemical stability insinuating as a promising candidate for photocatalytic and energy harvesting applications. Growth of a free standing film is desirable for widespread electronic devices and electrochemical applications. Here we present a facile approach to prepare free-standing films (15mm × 10mm × 0.5mm) comprising of g-C_3N_4 nanolayers by the pyrolysis of dicyandiamide ($C_2H_4N_4$) utilizing a chemical vapor deposition (CVD) technique. The synthesis is done under low-pressure conditions of Argon (~ 3 Torr) and at a temperature of 600 ^{0}C. The as-synthesized g-C_3N_4 films are systematically studied for their structural/microstructural characterization by using X-ray diffraction (XRD), scanning & transmission electron microscopy (SEM and TEM), X-ray photoelectron spectroscopy (XPS), Fourier transform infrared spectroscopy (FTIR) and UV-visible spectroscopy techniques. Excitation dependent photoluminescence (PL) spectra of the as-synthesized g-C_3N_4 film exhibit an intense, stable and broad emission peak in the visible region ~ 459 nm. The free standing g-C_3N_4 films emission spectra shows a blue shift and band sharpening as compared to the g-C_3N_4 powder.

Keywords: graphitic carbon nitride film; g-C_3N_4; spray pyrolysis; free-standing; fluorescence; emission

*** Corresponding authors:** rmanohar28@gmail.com (Dr. R.M. Yadav)
amarti@rice.edu (Prof. A.A. Martí)
ajayan@rice.edu (Prof. P.M. Ajayan)

1. Introduction

Ever since the discovery of graphene, two-dimensional (2D) materials have attracted intense scientific attention due to their striking new properties and promising diverse applications in various research areas and in the fabrications of new devices. Among these, graphene-like g-C_3N_4 nanostructures are promising for various applications due to their unique optical and electrical properties[1-3]. The π-conjugated graphitic planes in g-C_3N_4 structures originate from the carbon and nitrogen atoms linked via sp^2 hybridization [4]. The graphene-like layered g-C_3N_4 nanomaterial is composed of two basic structure units: s-triazine and tri-s-triazine (heptazine), and is typically nontoxic and metal-free [5-8]. This material exhibits outstanding physical and chemical properties[5-8] and is considered one of the best stable allotrope among various carbon nitrides under ambient conditions [9]. As an organic polymeric semiconductor, g-C_3N_4 has attracted worldwide interest due to a band-gap of ~2.7 eV and its adequate band-positions (delocalized electron states) for various redox reactions [10]. The 2D g-C_3N_4 nanomaterials own good biocompatibility, high fluorescence quantum yield, high chemical stability and good photocatalytic properties [11-17].

The g-C_3N_4 layered materials are usually prepared by a high-temperature pyrolysis process of carbon and nitrogen-rich organic compounds, such as urea (CH_4N_2O) [18], thiourea (CH_4N_2S)[19], cyanuric chloride ($C_3Cl_3N_3$)[20], dicyandiamide ($C_2H_4N_4$) [21, 22], ammonium thiocyanate (NH_4SCN) [23], melamine ($C_3H_6N_6$) [24, 25], cyanamide (CH_2N_2) [26], and ethylenediamine ($C_2H_8N_2$) with carbon tetrachloride, etc. Single layered to few layered g-C_3N_4 nanosheets were also synthesized by bulk g-C_3N_4 powder using a top-down approach. Niu et al. [27] reported a controllable thermal oxidation to etch bulk g-C_3N_4 into a few atomic layers that revealed superior photocatalytic activity. For example, Xu et al. [28] developed an H_2SO_4-intercalation method to synthesize single-layered g-C_3N_4 nanosheets and obtained a 3-fold enhancement in photocatalytic H_2 evolution. Also, Zhou et al. [29] reported a low-temperature solid-phase method to synthesize highly fluorescent C_3N_4 dots with a quantum yield of 42% from urea and sodium citrate, and Barman et al. [30] reported a microwave mediated method to prepare highly fluorescent g-C_3N_4 quantum dots with a quantum yield of 29% in formamide.

The g-C_3N_4 can have fascinating applications in many areas of basic science and technology. Particularly, it has significant applications for device fabrication in various fields, such as biosensing, bioimaging, ions detection, photocatalysis, optoelectronic devices, carbon dioxide reduction, water splitting and photodegradation of water pollutants [31-36]. Zhang et al. [37]

reported a pathway to prepare ultrathin g-C_3N_4 nanosheets for bioimaging by a liquid exfoliation route from bulk g-C_3N_4. Xu et al. [38] demonstrated the synthesis of ultrathin g-C_3N_4 films supported on attapulgite nanofibers for visible-light photocatalytic activity by degradation of methyl orange. In other applications, Rong et al. [39] developed an effective and facile fluorescence sensing approach for the selective determination of Cr(VI) using g-C_3N_4 nanosheets. Recently, the visible photoluminescence (PL) of carbon nitride bulk and nanopowder have been thoroughly studied. Zhang et al. [1] reported how the photoluminescence maximum of g-C_3N_4 nanopowder varied with growth parameters and proposed a luminescent mechanism. Zhao et al. [40] studied the photoluminescence behavior of functionalized g-C_3N_4 nanosheets grafted with rare earth metal nanoparticles, nonetheless an extensive photoluminescence study of pristine g-C_3N_4 nanolayers and their contrast with the bulk materials is highly desirable to understand the PL phenomenon of these nanomaterials and to make it available for different device applications.

In the present work, we report a simple and one step chemical vapor deposition (CVD) approach to synthesize free-standing g-C_3N_4 films. The free-standing g-C_3N_4 film was fabricated from thermal condensation of $C_2H_4N_4$ at 600 ^oC in a low pressure Ar atmosphere. We thoroughly characterized the g-C_3N_4 free standing films using spectroscopic techniques (particularly steady-state and time-resolve photoluminescence), XRD, TEM & SEM and further compared this material with the g-C_3N_4 powder spectra.

2. Experimental details

2.1. Synthesis of free-standing g-C_3N_4 films and powder

The synthesis of free-standing g-C_3N_4 films was carried out using a pyrolysis-assisted CVD method. In pyrolysis-assisted CVD, the dicyandiamide ($C_2H_4N_4$) powder was used as C and N source precursor and placed in a quartz tube towards the inlet of Ar gas flow. The outlet of the quartz tube was connected to a vacuum pump to maintain the low pressure (~3 Torr) inside the tube. Due to Ar gas flow with the low vacuum inside the quartz tube, the vapors of $C_2H_4N_4$ powder enter inside the hot zone of the furnace (600 ^oC). The condensation of $C_2H_4N_4$ at high temperature produces the g-C_3N_4 structure deposited inside the quartz tube. After deposition, the furnace was allowed to cool down to room temperature automatically under Ar ambient. A uniform yellow deposition inside the quartz tube at the reaction hot zone was observed (**Fig. 1**). The yellow deposition was collected in the form of a free-standing film which was analyzed further by using

different characterization techniques for structural and optical properties. The g-C_3N_4 powder was synthesized using the same precursors of dicyandiamide ($C_2H_4N_4$) at 600 ^{0}C in air atmosphere.

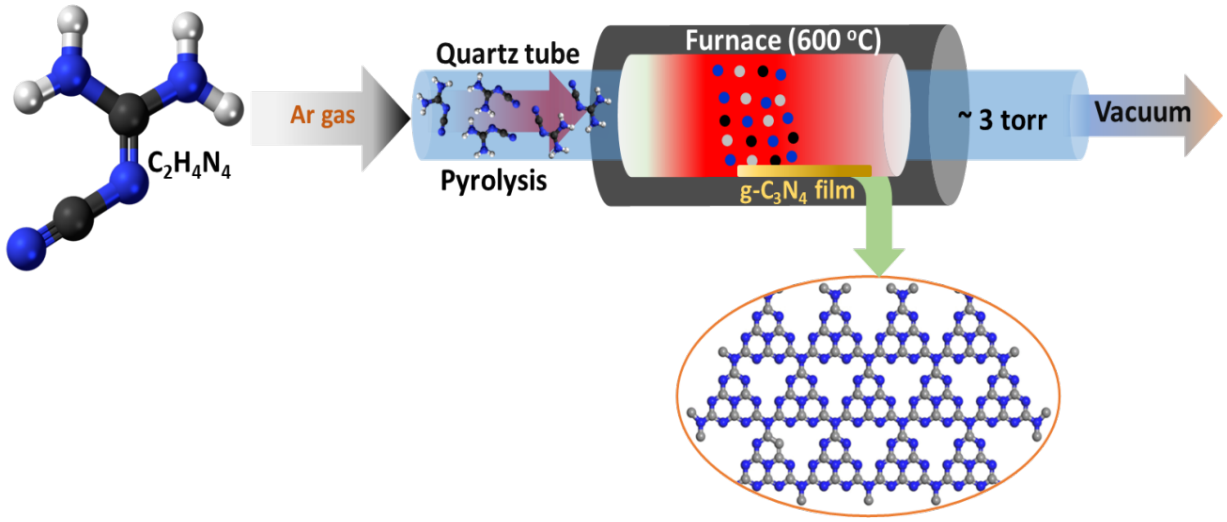

Fig. 1 Schematic representation of pyrolysis-assisted CVD synthesis for free-standing g-C_3N_4 films.

2.2. Characterization

The structural/microstructural and optical characterizations were performed via powder XRD, SEM, TEM, XPS, FTIR, UV-visible absorption and emission spectroscopy. The morphological and structural analyses of the synthesized samples were determined by SEM (FEI Quanta 400 FEG ESEM), TEM (JEOL 2100 FEG TEM) and XRD (Rigaku Smart Lab XRD). FTIR spectra were recorded by using a Nicolet FTIR Infrared Microscope. XPS system from PHI Quantera XPS (on a PHI-5000C ESCA system with Al Kα) was used for stoichiometric analysis. UV-visible absorption spectra were obtained using Shimadzu UV-2450 spectrophotometer. Steady-state fluorescence experiments were performed in a HORIBA Jovin Yvon Fluorolog 3 fluorometer and time-resolved experiments in an Edinburgh Instruments OD470 single-photoncounting spectrometer with a 372 nm picosecond pulse diode laser and a high-speed red detector.

3. Results and discussion

Fig. 2a shows the optical image of free-standing g-C_3N_4 film of approximate area ~150 mm^2 with the thickness about 0.5 mm (*l=15mm; w=10mm; t=0.5mm*). **Figs. 2b-e** show the SEM images of g-C_3N_4 film at different magnifications. As shown in **Fig. 2b and Fig. 2c,** the synthesized g-C_3N_4 film exhibited the nanosheet structures with top surfaces containing porous morphology with

wrinkled flakes. The high magnification images (**Fig. 2d and Fig. 2e**) show the nanoporous structures of g-C_3N_4 film, as marked by arrows.

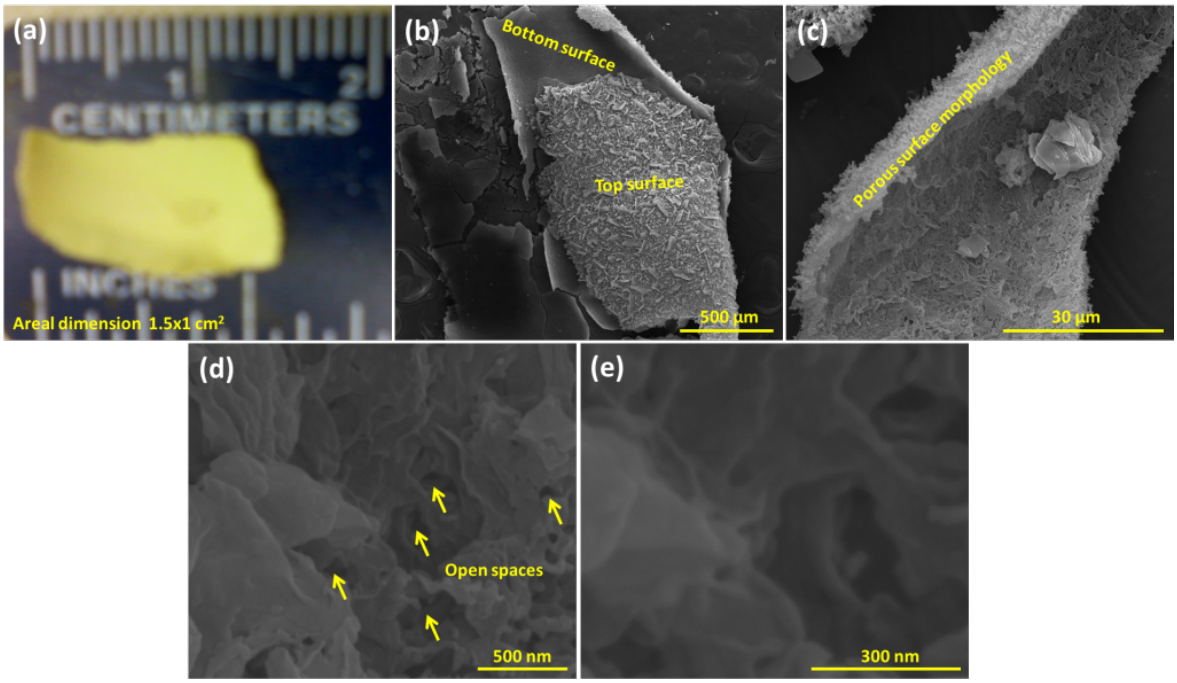

Fig. 2 Optical image (a) and SEM images (b-e) of as grown free-standingg-C_3N_4 films. SEM images are taken at different magnifications.

The detailed morphology of the free-standing g-C_3N_4 films was also investigated by TEM analysis (**Fig. 3a-c**), which confirmed their 2D structure and low thicknesses up to ~3nm. The g-C_3N_4 nanolayers exhibited sheets-like morphology with lengths up to several nanometers and of variable thicknesses as shown by arrows (**Fig. 3a**). In order to further examine the structure, high-resolution TEM (HRTEM) analysis was employed. Fig. 3b clearly revealed that the thickness of the g-C_3N_4 nanolayers is non-uniform. The different number of layers can be predicted due to the contrast variation (separated by dotted regions) and indicated by thin and thick nanolayers in **Fig. 3b**. It can be expected that thick nanolayers structure are formed due to the folding of g-C_3N_4 nanolayers.

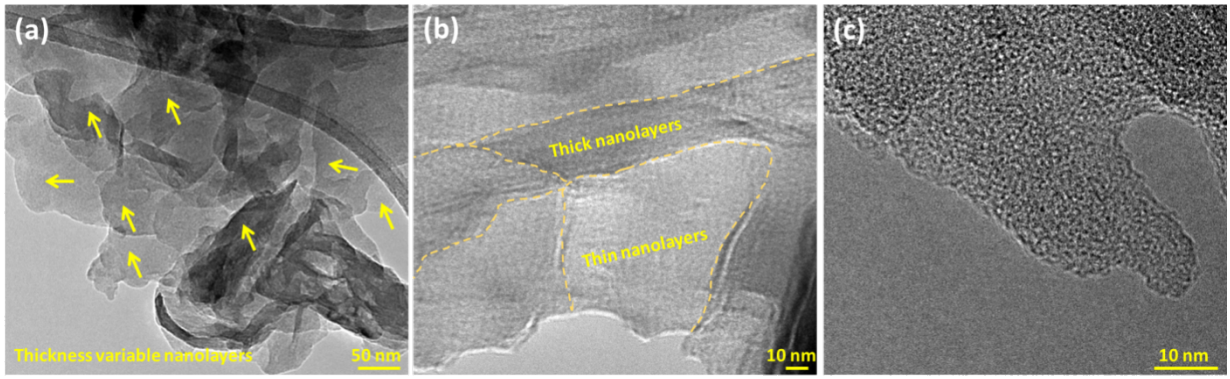

Fig. 3 TEM (a) and HRTEM (b,c) images of g-C_3N_4 film.

In order to investigate the crystalline structure of the free-standing g-C_3N_4 films, the XRD pattern of g-C_3N_4 film was analyzed. The observed XRD pattern of the g-C_3N_4 film, as shown in **Fig. 4a**, displays two diffraction peaks at 12.24° and 27.24° that correspond to the (100) and (002) planes of g-C_3N_4 respectively. This indicate the graphite-like inter-planar stacking of the conjugated aromatic units of CN that are the characteristic stacking structures of graphitic-like materials (hexagonal g-carbon nitride) (JCPDS card no. 87-1526) [41, 42]. We observed the same strong diffraction peaks from all the samples prepared, which indicates that free-standing g-C_3N_4 films with stable crystalline structure were successfully prepared from the pyrolysis of $C_2H_4N_4$.

In addition to X-ray diffraction analysis, FT-IR spectroscopy was used to characterize the chemical structure. A typical FT-IR spectrum of the free-standing g-C_3N_4 film is shown in **Fig. 4b**. Several bands are displayed in the region of 4000-700 cm^{-1}, which are characteristic of the C-N stretching. The sharp and intense transmittance band at 817 cm^{-1} can be attributed to the vibration of triazine rings, indicating the existence of the units with -NH and -NH_2 groups [43]. The several peaks in the region from 1200 to 1600 cm^{-1} can be attributed to typical stretching modes of either trigonal C-N (-C)-C or bridging C-NH-C units in g-C_3N_4 film [44, 45]. The broad peaks between 3070 and 3285 cm^{-1} correspond to N-H and O-H stretching and hydrogen-bonding interactions [32, 44].

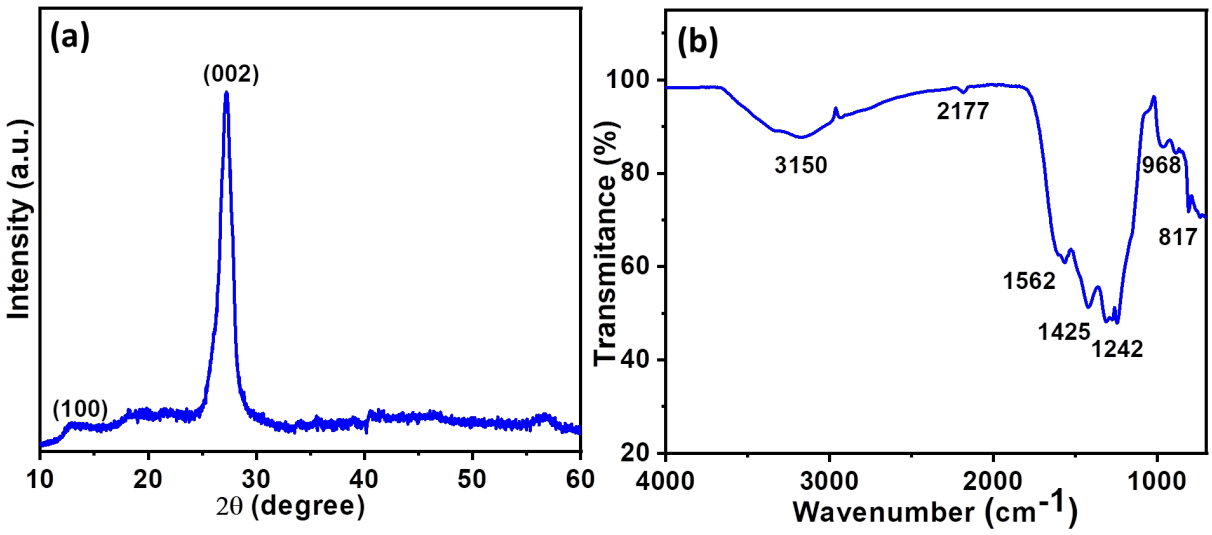

Fig. 4 (a) XRD pattern and (b) FT-IR spectra g-C_3N_4 film.

The XPS technique is well recognized and has been extensively utilized to provide binding energy of core level electrons of atoms in the solid. **Fig. 5a**, shows the C1s spectrum of a free-standing g-C_3N_4 film, which shows two broad peaks. These two deconvoluted peaks at 284.9 and 288.2 eV correspond to sp^2 C-C and sp^2 N-C=N bonds, respectively. The high-resolution N1s spectrum as shown in **Fig. 5b** has been deconvoluted into three peaks at 398.6, 399.9 and 401.0 eV, which were assigned to the sp^2-hybridized N (C-N-C), sp^3-hybridized N (tertiary N, (N-[C]$_3$) and amino functional groups with H atom (C-N-H), in that order [5, 43, 46-48]. These XPS results confirm that the basic substructure of the synthesized material is the heptazine heterocyclic ring unit.

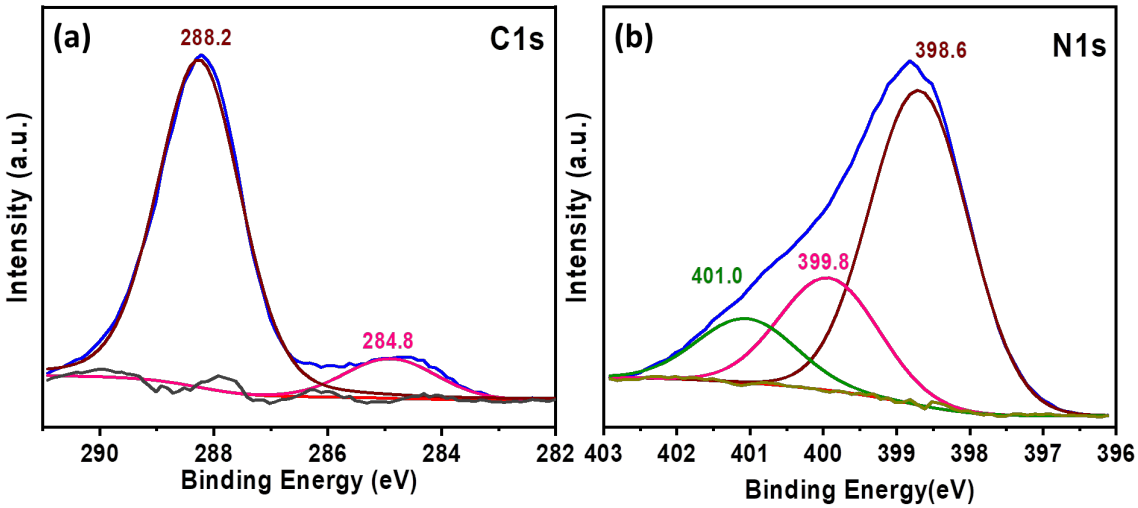

Fig. 5 High-resolution (a) C1s and (b) N1s XPS spectra of g-C_3N_4 film.

Fig. 6 displays the diffuse reflectance and fluorescence spectra of as-synthesized free-standing g-C_3N_4 film and g-C_3N_4 powder. **Fig. 6a** shows the diffuse reflectance spectrum of g-C_3N_4 film and g-C_3N_4 powder. The g-C_3N_4 film absorbed visible light up to ~470 nm, suggesting that it could be activated by visible light which is favorable for bio-imaging. [49, 50] Diffuse reflectance spectra has been commonly used as standard technique to estimate the band gap of semiconducting materials [51,52, 53]. The band gap for the samples can be calculated according to the following relation

$$F(R)h\nu = A(h\nu - E_g)^{\frac{n}{2}} \quad \ldots\ldots\ldots 1$$

$$Where\ F(R) = (1-R)^2/2R \ldots\ldots\ldots\ldots\ldots\ldots\ldots 2$$

- *F(R) is the* Kubelka–Munk (K–M) function.

In the equation, *n* equals to 1 or 4, depending on whether the transition is direct or indirect, respectively. X. Wang et al[54] showed that g-C_3N_4 has a non-isotropic band structure with a direct bandgap at the Γ point and only dispersion along the Γ–X direction parallel to the chain. There are reports suggesting direct[5] as well as indirect[16] band gap for g-C_3N_4. Here we are discussing the direct band gap although we have calculated the direct as well as indirect band gap for g-C_3N_4 films and powder (Fig. S1 a, b). The values of E_g for free-standing g-C_3N_4 film and g-C_3N_4 powder are calculated to be 2.86 and 2.70 eV, respectively (Fig. S1 a, b).The blue shift of the absorption edge and increasing of E_g value for g-C_3N_4 film as compared to that of g-C_3N_4 powder could be ascribed to the quantum confinement effects [21, 27, 55]. Fig. 6b shows the fluorescence spectra of the g-C_3N_4 film and g-C_3N_4 powder. It can be seen that the PL emission band of g-C_3N_4 film has a significant blue shift and also shows a narrower band profile with respect to that of g-C_3N_4 powder. This clearly suggests that g-C_3N_4 films contain relatively uniform particle size distribution as compared to that in g-C_3N_4 powder [29].

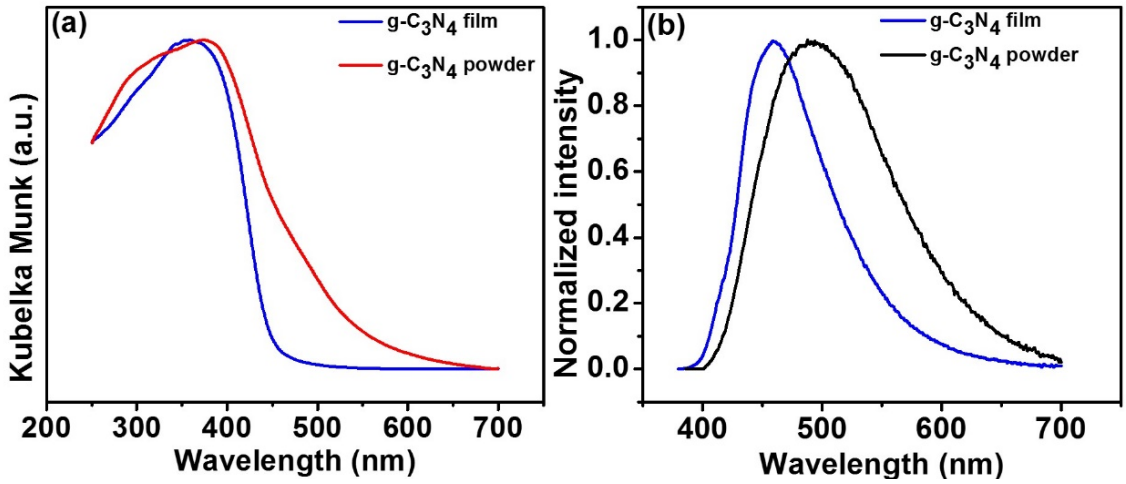

Fig. 6 (a) Diffuse reflectance spectra, and (b) PL spectra of g-C_3N_4 film and g-C_3N_4 powder.

Fig. 7a presents the excitation-dependent PL spectrum of free-standing g-C_3N_4 films. Various excitation wavelengths in the range of 300-424 nm were used to study the fluorescence emission spectrum. As expected, the fluorescent spectrum shows that the emission band (~ 450-460 nm) remains unchanged for all excitation wavelengths. Nonetheless, the PL emission peak intensity varies with excitation wavelength as shown in **Fig. 7b**. It was found to increase with increasing the excitation wavelength with maximum intensity at 372 nm. The constant emission wavelength band (450-460 nm) from all the synthesized free-standing g-C_3N_4 films indicate that the g-C_3N_4 films are optically similar. Also, the films show high photostability, with the fluorescence intensity remaining constant after continuous irradiation.

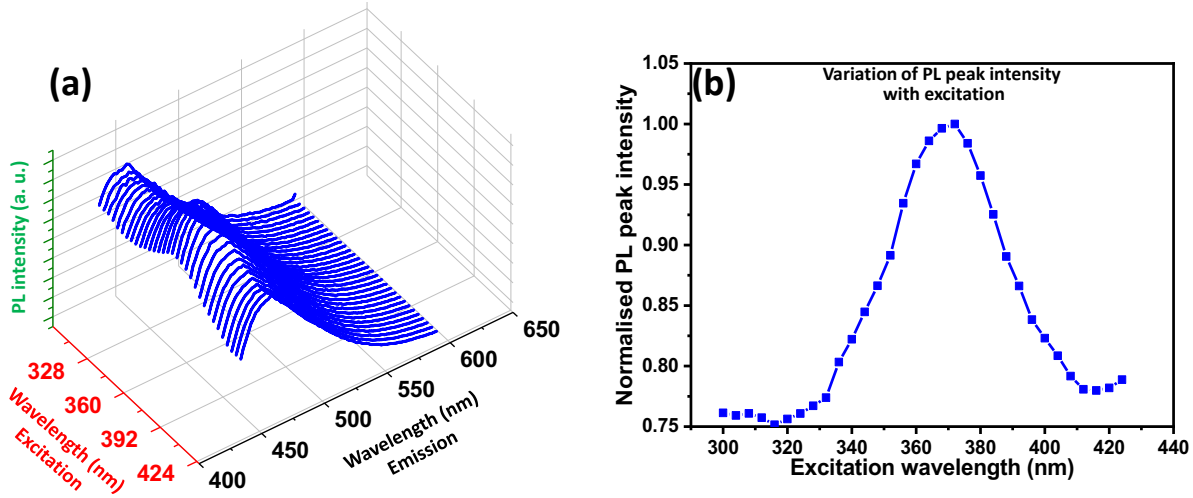

Fig. 7 (a) Excitation-dependent fluorescence emission spectrum (excitation wavelengths changes from 300 nm to 424 nm) and (b) variation of emission intensity of g-C_3N_4 film with excitation wavelength at emission 459 nm.

To compare the results with g-C_3N_4 film, we have also studied the PL emission spectra of g-C_3N_4 powder. **Fig. S2** shows the excitation dependent PL emission spectra of g-C_3N_4 powder. The maximum PL intensity was found around 488 nm with excitation wavelength 330 nm. The PL emission profiles of g-C_3N_4 powder and g-C_3N_4 film are shown in **Fig. S3**. The emission profiles clearly illustrate the difference in emission from g-C_3N_4 powder and g-C_3N_4 film. This plot reveals that the emission profile of g-C_3N_4 film is relatively narrow (**Fig. S3(a)**), while in the case of g-C_3N_4 powder the band is broader (**Fig. S3(b)**). Overall analysis obtained from the absorption and emission in the visible region, suggests that free-standing g-C_3N_4 film can be used for a variety of applications from solar energy conversion to bio-imaging applications.

Fig. 8 shows the fluorescence decay curve of the g-C_3N_4 film using 372 nm excitation wavelength with instrument response function (IRF) and multi exponential fit curve. The decay curve clearly shows the deviation from the single-exponential decay, which indicates that multiple environments are represented in the emission profile [56]. By the multi-exponential fitting, the fluorescence lifetimes of the free-standing g-C_3N_4 film were found to be about 27 ns, 120 ns and 90 ns. The nanosecond lifetime of g-C_3N_4 films endows their potential applications in bio-imaging[37, 57] displays, lighting[58], etc. Bayan et al.[58] reported the white luminescence from heterojunctions based on two dimensional (2D) graphitic carbon nitride (g-C_3N_4) nanosheets and ZnO nanorods and shows the applicability of g-C_3N_4 in white light emission. Jia et al[59] synthesized the free standing super hydrophilic g-C_3N_4 film and reported their excellent performance, stability and recyclability for the catalytic dye degradation. Xie et al[60] reported the in- situ growth of g-C_3N_4 films on transparent substrate by solvothermal method. Their results revealed that g-C_3N_4 films are convenient for photo electrochemical energy conversion

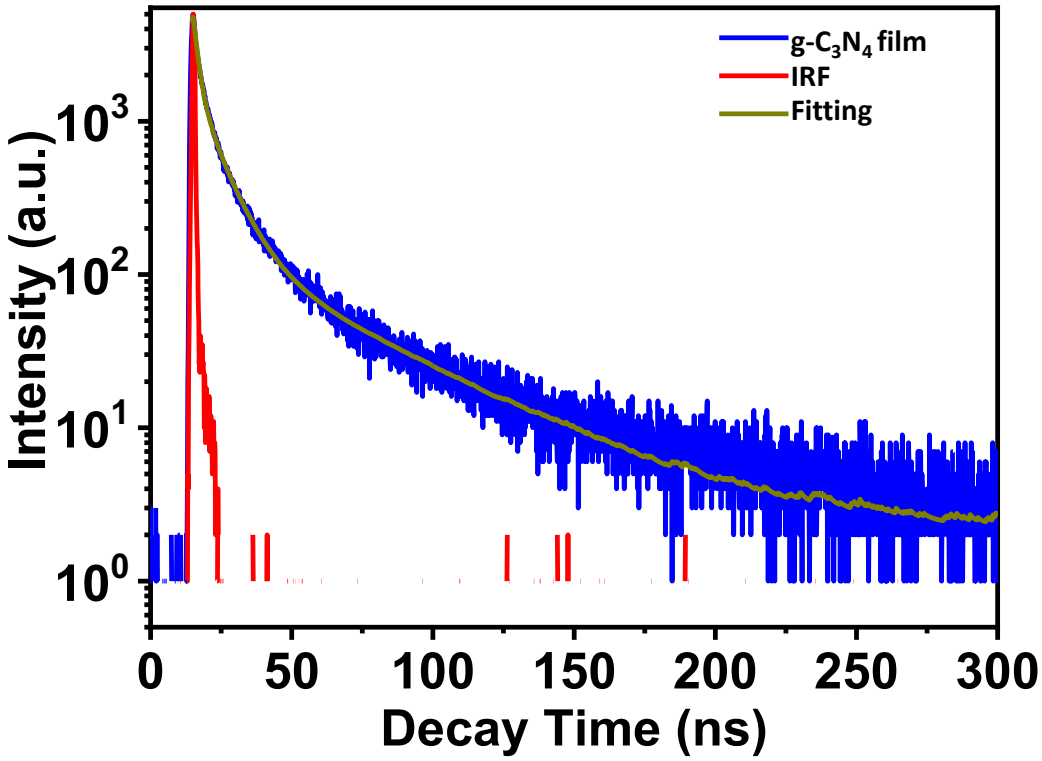

Fig. 8 Decay curve of g-C_3N_4 free standing film with multi exponential fitting and IRF curve.

Fig. 9 shows the transient PL spectra of g-C_3N_4 powder and g-C_3N_4 films. The emission intensities of these peaks exponentially decrease with increasing the decay time. The transient PL emission spectra of g-C_3N_4 film (Fig. 9a) exactly correlates with the finding of excitation-dependent fluorescence emission spectrum (Fig. 7) however transient PL emission spectra of g-C_3N_4 powder (Fig. 9b) reveal two peaks at 480 nm and 525 nm as compared to one broad peak of fluorescence emission spectrum at 489 nm (Fig. S2 & S3b). The reason of two peaks in transient spectra is not clear but Zhang et al[1] suggested that the obvious difference between the steady-state and transient PL emission spectra implies that there is more than one PL emission center during the emission process of carbon nitride powder and it seems that these two peaks merged in one peak in PL spectra of g-C_3N_4 powder. The PL emission spectra of the g-C_3N_4 film show the single sharper peak as compared to g-C_3N_4 powder. It is clearly evident that during emission process more PL emission centers are present in g-C_3N_4 powder as compared to g-C_3N_4 films.

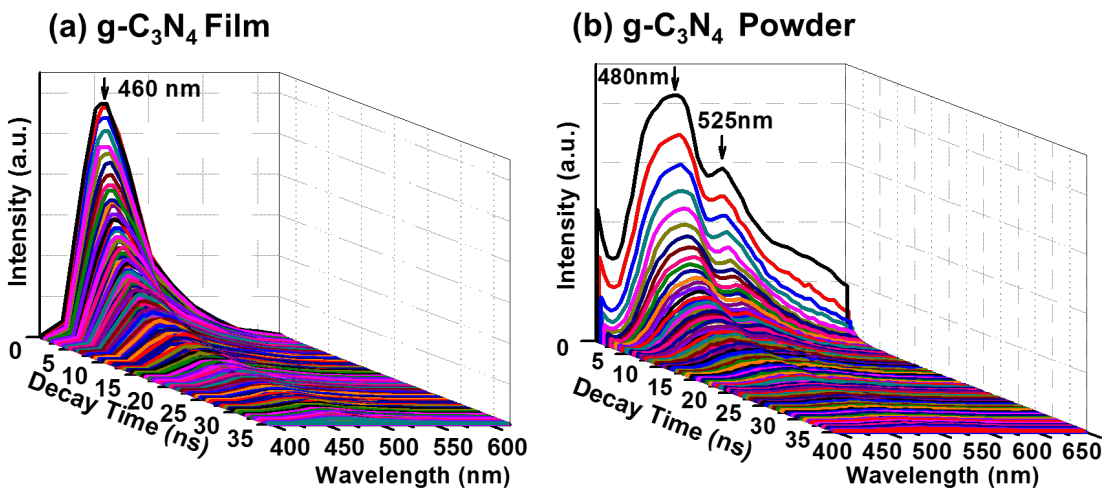

Fig. 9 Time resolved PL emission spectra of (a) g-C_3N_4 film and (b) g-C_3N_4 powder.

The blue shift for PL emission in g-C_3N_4 films could be attributed to quantum confinement effects arising due to smaller particle size in g-C_3N_4 films as compared to powder initiating the band gap to widen up [28]. It is evident from the XRD and XPS spectra, the g-C_3N_4 free standing films consisted of heptazine structure[61] which has higher disorder and delocalization of electrons. Zhang et al. [1] revealed that the delocalization of electrons and thus overlap of orbitals leads to vanishing or weaken the transition probability between Π and Π* states [62, 63] and thus the peaks at 525 nm disappears in g-C_3N_4 films.

4. Conclusions

In summary, we have developed a facile one-step CVD assisted approach for the synthesis of high-quality and large area (15mm×10mm) free-standing g-C_3N_4 films by direct pyrolysis of $C_2H_4N_4$ in a quartz tube at 600 ^{0}C. The film was made up of g-C_3N_4 nanolayers with variable thickness due to folding and overlapping of various nanolayers. The detailed PL spectra and decay analysis obtained with different excitation energies revealed no significant change in the position of the emission band and hence confirms the existence of a particular energy band. The as-synthesized g-C_3N_4 film exhibited stable and strong photoluminescence emission centered around 455-460 nm. The photoluminescence lifetime analysis as detected from the time decay spectra suggest this free-standing g-C_3N_4 film as a prospective candidate for bioimaging and display applications. This simple approach can be expanded for the synthesis and creation of stable polymeric g-C_3N_4 film with various microstructures.

Acknowledgements

RMY acknowledges USIEF & Fulbright Commission for Fulbright Nehru Academic and Professional Excellence Fellowship. AAM thanks NSF CHE 1807737 for financial assistance. R. Kumar acknowledges Japan Society for the Promotion of Science (JSPS; Standard) for international postdoctoral fellowship (P18063) and financial supported by JSPS KAKENHI Grant No.18F18063.

References

1. Y. Zhang, Q. Pan, G. Chai, M. Liang, G. Dong, Q. Zhang and J. Qiu, *Sci Rep*, 2013, **3**, 1943.
2. J. Liu, H. Wang and M. Antonietti, *Chem Soc Rev*, 2016, **45**, 2308-2326.
3. W. J. Ong, L. L. Tan, Y. H. Ng, S. T. Yong and S. P. Chai, *Chem Rev*, 2016, **116**, 7159-7329.
4. L. Chen, D. Huang, S. Ren, T. Dong, Y. Chi and G. Chen, *Nanoscale*, 2013, **5**, 225-230.
5. A. Thomas, A. Fischer, F. Goettmann, M. Antonietti, J.-O. Müller, R. Schlögl and J. M. Carlsson, *Journal of Materials Chemistry*, 2008, **18**, 4893-4908.
6. M. Deifallah, P. F. McMillan and F. Corà, *The Journal of Physical Chemistry C*, 2008, **112**, 5447-5453.
7. G. M. and A. M., *Advanced Materials*, 2005, **17**, 1789-1792.
8. A.-S. Gerardo, S. Nikolai, C. S. Y., B. Torbjörn, P. R. G., L. Andrea, A. Markus, K. Y. Z., K. A. V., R. J. P., K. Ute, C. A. I., T. Arne and B. M. J., *Angewandte Chemie International Edition*, 2014, **53**, 7450-7455.
9. S. Cao and J. Yu, *The Journal of Physical Chemistry Letters*, 2014, **5**, 2101-2107.
10. G. Frederic, F. Anna, A. Markus and T. Arne, *Angewandte Chemie International Edition*, 2006, **45**, 4467-4471.
11. G. Shiravand, A. Badiei and G. Mohammadi Ziarani, *Sensors and Actuators B: Chemical*, 2017, **242**, 244-252.
12. J.-W. Liu, Y. Luo, Y.-M. Wang, L.-Y. Duan, J.-H. Jiang and R.-Q. Yu, *ACS Applied Materials & Interfaces*, 2016, **8**, 33439-33445.
13. M. Xiong, Q. Rong, H.-m. Meng and X.-b. Zhang, *Biosensors and Bioelectronics*, 2017, **89**, 212-223.
14. Q. Zhuang, L. Sun and Y. Ni, *Talanta*, 2017, **164**, 458-462.
15. M.-H. Xiang, J.-W. Liu, N. Li, H. Tang, R.-Q. Yu and J.-H. Jiang, *Nanoscale*, 2016, **8**, 4727-4732.
16. S. Zuluaga, L.-H. Liu, N. Shafiq, S. M. Rupich, J.-F. Veyan, Y. J. Chabal and T. Thonhauser, *Physical Chemistry Chemical Physics*, 2015, **17**, 957-962.
17. Q. Lu, J. Deng, Y. Hou, H. Wang, H. Li and Y. Zhang, *Chemical Communications*, 2015, **51**, 12251-12253.
18. F. Dong, L. Wu, Y. Sun, M. Fu, Z. Wu and S. C. Lee, *Journal of Materials Chemistry*, 2011, **21**, 15171-15174.
19. F. Dong, Y. Sun, L. Wu, M. Fu and Z. Wu, *Catalysis Science & Technology*, 2012, **2**, 1332-1335.
20. C. Li, C.-B. Cao, H.-S. Zhu, Q. Lv, J.-T. Zhang and X. Xiang, *Materials Science and Engineering: B*, 2004, **106**, 308-312.
21. H.-Y. Xu, L.-C. Wu, H. Zhao, L.-G. Jin and S.-Y. Qi, *PLOS ONE*, 2015, **10**, e0142616.
22. L. Song, S. Zhang, X. Wu and Q. Wei, *Chemical Engineering Journal*, 2012, **184**, 256-260.
23. Y. Cui, J. Huang, X. Fu and X. Wang, *Catalysis Science & Technology*, 2012, **2**, 1396-1402.
24. H. Montigaud, B. Tanguy, G. Demazeau, I. Alves and S. Courjault, *Journal of Materials Science*, 2000, **35**, 2547-2552.
25. L. Ge, *Materials Letters*, 2011, **65**, 2652-2654.

26. K. Maeda, X. Wang, Y. Nishihara, D. Lu, M. Antonietti and K. Domen, *The Journal of Physical Chemistry C*, 2009, **113**, 4940-4947.
27. N. Ping, Z. Lili, L. Gang and C. Hui-Ming, *Advanced Functional Materials*, 2012, **22**, 4763-4770.
28. J. Xu, L. Zhang, R. Shi and Y. Zhu, *Journal of Materials Chemistry A*, 2013, **1**, 14766-14772.
29. J. Zhou, Y. Yang and C.-y. Zhang, *Chemical Communications*, 2013, **49**, 8605-8607.
30. S. Barman and M. Sadhukhan, *Journal of Materials Chemistry*, 2012, **22**, 21832-21837.
31. Y. Tang, H. Song, Y. Su and Y. Lv, *Analytical Chemistry*, 2013, **85**, 11876-11884.
32. Q. Han, B. Wang, J. Gao, Z. Cheng, Y. Zhao, Z. Zhang and L. Qu, *ACS Nano*, 2016, **10**, 2745-2751.
33. D. Das, S. L. Shinde and K. K. Nanda, *ACS Applied Materials & Interfaces*, 2016, **8**, 2181-2186.
34. J. J. Walsh, C. Jiang, J. Tang and A. J. Cowan, *Physical Chemistry Chemical Physics*, 2016, **18**, 24825-24829.
35. S. C. Yan, Z. S. Li and Z. G. Zou, *Langmuir*, 2009, **25**, 10397-10401.
36. J. Zhu, P. Xiao, H. Li and S. A. C. Carabineiro, *ACS Applied Materials & Interfaces*, 2014, **6**, 16449-16465.
37. X. Zhang, X. Xie, H. Wang, J. Zhang, B. Pan and Y. Xie, *Journal of the American Chemical Society*, 2013, **135**, 18-21.
38. Y. Xu, L. Zhang, M. Yin, D. Xie, J. Chen, J. Yin, Y. Fu, P. Zhao, H. Zhong, Y. Zhao and X. Wang, *Applied Surface Science*, 2018, **440**, 170-176.
39. M. Rong, L. Lin, X. Song, Y. Wang, Y. Zhong, J. Yan, Y. Feng, X. Zeng and X. Chen, *Biosensors and Bioelectronics*, 2015, **68**, 210-217.
40. Y. Zhao, R. Wei, X. Feng, L. Sun, P. Liu, Y. Su and L. Shi, *ACS Applied Materials & Interfaces*, 2016, **8**, 21555-21562.
41. S. Li, G. Dong, R. Hailili, L. Yang, Y. Li, F. Wang, Y. Zeng and C. Wang, *Applied Catalysis B: Environmental*, 2016, **190**, 26-35.
42. L. Shi, L. Liang, F. Wang, M. Liu, S. Zhong and J. Sun, *Catalysis Communications*, 2015, **59**, 131-135.
43. X. Li, G. Hartley, A. J. Ward, P. A. Young, A. F. Masters and T. Maschmeyer, *The Journal of Physical Chemistry C*, 2015, **119**, 14938-14946.
44. N. Rahbar, P. Abbaszadegan and A. Savarizadeh, *Analytica Chimica Acta*, 2018, **1026**, 117-124.
45. J. Xu and M. Shalom, *ACS Applied Materials & Interfaces*, 2016, **8**, 13058-13063.
46. J. Biechele-Speziale, B. T. Huy, T. T. T. Nguyen, N. M. Vuong, E. Conte and Y.-I. Lee, *Microchemical Journal*, 2017, **134**, 13-18.
47. W.-J. Ong, L.-L. Tan, S.-P. Chai, S.-T. Yong and A. R. Mohamed, *Nano Energy*, 2015, **13**, 757-770.
48. Y. Zhang, J. Liu, G. Wu and W. Chen, *Nanoscale*, 2012, **4**, 5300-5303.
49. L. Wang, Y. Yin, A. Jain and H. S. Zhou, *Langmuir*, 2014, **30**, 14270-14275.
50. P. Hu, C. Chen, R. Zeng, J. Xiang, Y. Huang, D. Hou, Q. Li and Y. Huang, *Nano Energy*, 2018, **50**, 376-382.
51. R. López and R. Gómez, *Journal of Sol-Gel Science and Technology*, 2012, **61**, 1-7.
52. B. Karvaly and I. Hevesi, *Journal*, 1971, **26**, 245.
53. W. Klockner, R. M. Yadav, J. Yao, S. Lei, A. Aliyan, J. Wu, A. A. Martí, R. Vajtai, P. M. Ajayan, J. C. Denardin, D. Serafini, F. Melo and D. P. Singh, 2017, **19**, 288.
54. X. Wang, K. Maeda, A. Thomas, K. Takanabe, G. Xin, J. M. Carlsson, K. Domen and M. Antonietti, *Nature Materials*, 2008, **8**, 76.
55. Y. Shubin, G. Yongji, Z. Jinshui, Z. Liang, M. Lulu, F. Zheyu, V. Robert, W. Xinchen and A. P. M., *Advanced Materials*, 2013, **25**, 2452-2456.
56. L. Xiaofeng, Y. Song, D. Guoping, Q. Yanbo, R. Jian, Z. Yixi, Z. Qiang, L. Geng, C. Danping and Q. Jianrong, *Journal of Physics D: Applied Physics*, 2009, **42**, 215409.
57. A. Wang, C. Wang, L. Fu, W. Wong-Ng and Y. Lan, *Nano-Micro Letters*, 2017, **9**, 47.
58. S. Bayan, N. Gogurla, A. Midya and S. K. Ray, *Carbon*, 2016, **108**, 335-342.

59. F. Jia, Y. Zhang, W. Hu, M. Lv, C. Jia and J. Liu, *Frontiers in Materials*, 2019, **6**.
60. X. Xie, X. Fan, X. Huang, T. Wang and J. He, *RSC Advances*, 2016, **6**, 9916-9922.
61. Y. Wang, X. Wang and M. Antonietti, *Angew Chem Int Ed Engl*, 2012, **51**, 68-89.
62. I. Yuta Iwano and Toshiaki Kittaka and Hidekazu Tabuchi and Masaya Soukawa and Shinsuke Kunitsugu and Kenichi Takarabe and Kunio, *Japanese Journal of Applied Physics*, 2008, **47**, 7842.
63. A. Du, S. Sanvito, Z. Li, D. Wang, Y. Jiao, T. Liao, Q. Sun, Y. H. Ng, Z. Zhu, R. Amal and S. C. Smith, *J Am Chem Soc*, 2012, **134**, 4393-4397.